IF 51 (286)
"FATIGUE CRACK
GROWTH BEHAVIOR"

FATIGUE CRACK GROWTH BEHAVIOR OF CARBON BLACK–REINFORCED NATURAL RUBBER

LEWIS B. TUNNICLIFFE

BIRLA CARBON, 1800 WEST OAK COMMONS COURT, MARIETTA, GA 30062

RUBBER CHEMISTRY AND TECHNOLOGY, Vol. 94, No. 3, pp. 494–514 (2021)

ABSTRACT

Fatigue crack growth behavior of carbon black–reinforced natural rubber is investigated. Rubber compounds of Shore A = 70 are prepared by varying the formulation loadings of a wide range of carbon black types based on their structure and surface area properties. The resulting fatigue crack growth behavior shows significant variation in β exponent values, depending on the properties of the carbon black. These variations are rationalized by considering the strain amplification of natural rubber by carbon black aggregates in the region of compound directly ahead of the crack tip. An assumption is made that little networking of the carbon black aggregates exists in this region of very high strain and that hydrodynamic calculations that consider occluded rubber can therefore provide realistic values for strain amplification. A reasonable scaling of power law crack growth parameters to calculated strain amplification factors is found, with the exponent, β, decreasing with increasing strain amplification. The implication here is that enhanced strain amplification promotes the formation of strain-induced crystallites in the crack tip region. Performance tradeoffs resulting from the crossover of crack growth data sets dependent on the carbon black type are discussed. Of practical significance is the fact that the strain amplification factors can be calculated directly from knowledge of carbon black type and loading in rubber formulations. [doi:10.5254/rct.21.79935]

INTRODUCTION

The fatigue life of rubber components is a critical performance parameter for engineering applications in which dynamic loading–unloading conditions are encountered and is most commonly discussed and understood in terms of the principles of fracture mechanics.[1–5] In its simplest form, the fatigue life of a rubber article can be defined by the operational time or number of loading cycles or events required for a crack to grow to a certain critical length after which catastrophic mechanical failure of the article occurs and/or the operational function of the article is compromised. This lifetime is governed by two principle effects:

1. The nucleation or initiation of cracks within the rubber article (or at the article surface) from crack precursors
2. The intrinsic crack growth resistance of the rubber compound, which defines the rate at which cracks originating from precursors can grow to the critical length required for catastrophic mechanical failure[1–6,8–10]

Reinforcing rubber with particulates such as carbon black (CB) plays a key role in extending the lifetime of rubber components. Reductions in fatigue crack growth (FCG) rates and an improved resistance to catastrophic tearing are characteristic features of CB reinforcement, but the exact mechanisms underpinning these phenomena are still incompletely understood. This article explores the role of CB in FCG of natural rubber and attempts to correlate the observed crack growth behavior to key characteristics of the CB and to propose microstructural toughening mechanisms. A brief background of the fracture mechanics of crack growth and tearing and of CB reinforcement of rubber is now presented.

Corresponding author. Email: Lewis.Tunnicliffe@adityabirla.com

สำเนาเพื่อใช้ในการศึกษาเท่านั้น

Downloaded from http://meridian.allenpress.com/rct/article-pdf/94/3/494/2908699/i0035-9475-94-3-494.pdf by Bureau of Science & Technology Information user on 06 October 2021

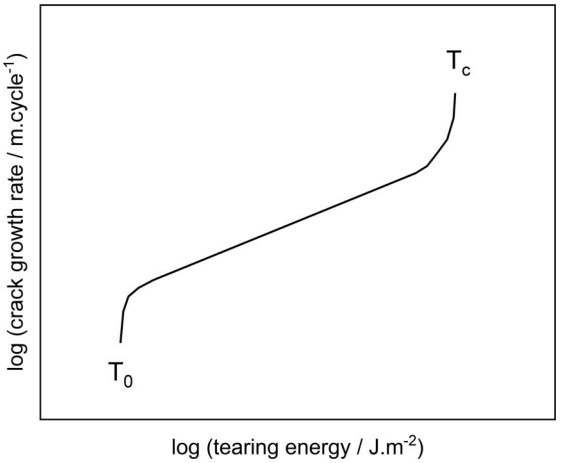

FIG. 1. — Schematic of intrinsic fatigue crack growth behavior.

FRACTURE MECHANICS APPROACH TO CRACK GROWTH

Crack growth behavior can be evaluated using a fracture mechanics approach by measuring the crack growth rate under fatigue loadings over a wide range of tearing energies. Tearing energy, T, refers to the strain energy released upon growth of a crack by area da, as defined in Eq. 1, where U is the strain energy in the rubber specimen.[11,12]

$$T = -\left(\frac{dU}{da}\right)_l \tag{1}$$

The tearing energy is theoretically independent of test piece geometry, and therefore, the resulting FCG data set is an intrinsic material characterization. Schematic FCG data are presented in Figure 1. The tearing energy below which no crack growth occurs is termed the *fatigue threshold*, T_0, and is typically of the order of 0.04–0.10 kJ/m^2.[9,10,13,14] At very high tearing energies, the failure process transitions from crack growth to catastrophic tearing.[15,16] The tearing energy at which this transition occurs is the critical tear energy, T_c, of the order of 10–50 kJ/m^2 for compounds typically used in tire applications. Crack growth rates for tearing energies between T_0 and T_c are commonly described by a power law relationship such as in Eq. 2, where c is the crack length, n is the number of fatigue cycles, and A and β are material-dependent parameters.[17]

$$\frac{dc}{dn} = AT^{\beta} \tag{2}$$

The selection of materials plays a critical role in controlling both T_c and power law crack growth behavior. Crack growth behavior is strongly influenced by localized hysteresis and microstructural morphology effects in the crack tip region and associated viscoelastic process zone. Local hysteresis acts to increase the total external work required before fracture can occur. Morphological features at the crack tip, such as localized strain-induced crystallization (SIC) in NR, acts to arrest and deflect the crack, thereby suppressing incremental crack growth.[18,19]

CB REINFORCEMENT AND CRACK GROWTH

The fundamental reinforcing unit of CB is the aggregate, which is composed of a fused assembly of paracrystalline primary particles with diameters of a few tens of nanometers. The size

Downloaded from http://meridian.allenpress.com/rct/article-pdf/94/3/494/2908699/i0035-9475-94-3-494.pdf by Bureau of Science & Technology Information user on 06 October 2021

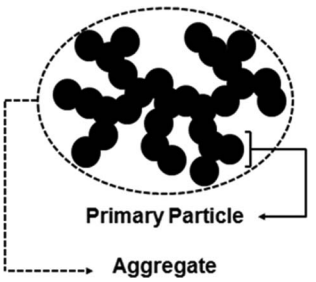

FIG. 2. — Schematic of the primary particle–aggregate hierarchical structure of carbon black.

of the primary particles dictates both the surface area of the CB and, to a large extent, the effective size of the aggregate. CB aggregates can also vary in their level of structure, which is essentially the number of primary particles comprising the aggregate and the degree of branching of the aggregate. This is schematically illustrated in Figure 2. An extensive body of literature on CB morphology is available for further details.[20,21]

Both the primary particle size and aggregate structure of CB control key aspects of rubber reinforcement. Aggregate structure defines the volume of rubber occluded from globally applied strains and contributes to the magnitude of strain amplification within the rubber, thereby controlling the static stiffness of the compound.[22] Aggregate structure is typically measured by oil absorption techniques.[23] By contrast, the primary particle size is the dominant factor defining the aggregate size and therefore the number of aggregates per unit volume of rubber compound. Consequently, the primary particle size has a dominant effect on dynamic stiffness and hysteresis. The surface area is typically measured using gas adsorption techniques.[24]

CB reinforcement significantly increases rubber compound durability over that of the gum unfilled material. The loading level of CB, in-rubber dispersion state, morphology, and particle size of the CB are all key parameters defining FCG and T_c performance. However, despite its undoubted practical significance, the role of CB in FCG performance is less well documented and understood than, for example, the effect of the rubber type. This can be partially attributed to the significant effort, equipment costs, and time required for extensive FCG characterization of a wide range of compounds. Previous studies have in general restricted their focus to just a few types of CB, typically at a fixed loading.

For example, the work of Lake and Lindley,[25] first reported in 1964 and reproduced extensively in the rubber literature,[1,4,26] surveyed the FCG performance of a wide range of different rubbers but only two variants of CB: N990 and N330. Rowlinson et al.[27] studied FCG in CB-reinforced SBR and observed variations in crack growth and tear behavior depending on the type and loading of CB in the compound. Le Cam et al.[6] studied the mechanisms of crack propagation in CB-reinforced NR and highlighted the role of cavity formation ahead of the crack tip. Reincke et al.[28] studied crack growth in various CB-reinforced SBR compounds and observed some dependence of the crack growth behavior on type and loading of CB. More recently, Wunde and Klüppel[29] discussed the role of CB networking and viscoelasticity on the crack growth resistance of SBR. Sridharan et al.[30] examined the influence of CB reinforcement on FCG resistance in compounds with various NR/BR blend ratios. Pilarski et al.[31] performed a comprehensive study of the fatigue life of CB-reinforced natural rubber, which indicated a complex interplay between crack precursor size and FCG behavior of the compounds. It has also been widely demonstrated that CB significantly increases the fatigue threshold, T_0, above that of the unfilled rubber.[1,9,14]

Downloaded from http://meridian.allenpress.com/rct/article-pdf/94/3/494/2908699/i0035-9475-94-3-494.pdf by Bureau of Science & Technology Information user on 06 October 2021

TABLE I
COLLOIDAL PROPERTIES OF CARBON BLACKS[a]

Carbon black	NSA, $m^2.g^{-1}$	STSA, $m^2.g^{-1}$	OAN, $mL.100g^{-1}$	COAN, $mL.100g^{-1}$
N990	8	8	38	37
N772	32	31	65	62
N660	35	34	90	75
N550	38	38	121	83
N326	77	77	72	73
N330	76	76	102	89
N339	91	88	120	99
CB1	25	25	45	43
CB2	25	25	95	68
CB3	28	27	127	83
CB4	60	55	143	99
CB5	106	104	60	55

[a] NSA, nitrogen surface area; STSA, statistical thickness surface area; OAN, oil absorption number; COAN, compressed oil absorption number.

Few quantitative correlations have been drawn between the fundamental properties of CB and FCG behavior. However, a general consensus on the roles of CB in FCG performance is now well established:

1. Local hysteresis in the viscoelastic process zone ahead of the crack tip imparted by the presence of CB requires the input of additional work to drive crack growth versus the corresponding unfilled material,
2. Filler-induced strain amplification in the crack tip region in crystallizing rubbers promotes the formation of strain-induced crystallites ahead of the crack, which retards crack growth rates.

Both of these mechanisms are well supported by experimental evidence but lack a quantitative and practical correlation to key CB properties. Reduced global onset strains for SIC in filled NR versus unfilled NR have been extensively demonstrated from various X-ray scattering experiments,[32] including observation of crystallization directly ahead of crack tips.[12] The effect of viscoelasticity (originating from both the rubber and from the filler network) in defining T_c is also very well established.[33]

The ultimate goal of this work is to provide a framework for rational selection of CB for maximum rubber compound crack growth and catastrophic tearing resistance, ideally derived from simple CB characteristics and rubber formulation information.

MATERIALS AND METHODOLOGIES

Twelve CB samples were selected to cover a wide range of surface area and structure combinations. All CBs were produced by Birla Carbon (Marietta, GA, USA), except the N990 material, which was produced by Cancarb (Medicine Hat, Alberta, Canada). Basic surface area and structure data for the CBs are given in Table I. The reported surface area values are the nitrogen surface area determined from Brunauer–Emmett–Teller (BET) analysis of nitrogen adsorption isotherms[23] and the statistical thickness surface area also determined from the nitrogen isotherms, which is a measure of the surface area of the CB accessible to the rubber macromolecules.[23] The

Downloaded from http://meridian.allenpress.com/rcl/article-pdf/94/3/494/2908699/i0035-9475-94-3-494.pdf by Bureau of Science & Technology Information user on 06 October 2021

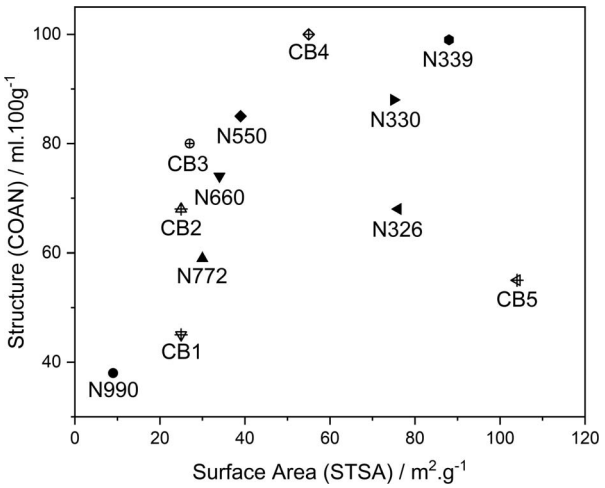

FIG. 3. — Colloidal plot of carbon blacks studied in this article. A measure of carbon black structure (COAN) is plotted versus a measure of surface area.

structure of the CBs is measured by oil absorption tests on the raw CB (oil absorption number; OAN)[24] and on precompressed CB (compressed oil absorption number; COAN).[24] The COAN structure level is thought to be more indicative of the structure level of CB after aggregate attrition from mixing with rubber.[24] The structure–surface area colloidal space for these CBs is plotted in Figure 3. All rubber compounds were prepared using the same basic NR formulation given in Table II. Compounds were prepared on a 1.6 L capacity Banbury mixer according to Table III. Cure properties were measured on an Alpha Technologies (Hudson, OH, USA) MDR device, and samples were vulcanized at 150 °C to a time of T_{90}+5 min based on the MDR data. Compound formulations varied only in CB type and loading. The macro-dispersion index of the CB in each compound was >90 by ASTM D2663 method D, indicating excellent macro-incorporation in each compound. Rubber compounds were prepared at iso-hardness. CB loadings were adjusted to match the hardness values of N550 loaded at 50 parts per hundred rubber (phr), which is ~70 Shore A. CB loadings required for iso-hardness are given in Table IV.

BASIC PHYSICAL PROPERTIES

The basic characterization of compound rheology and cure,[34] Shore A hardness,[35] rebound resilience,[36] and stress–strain behavior[37] was performed according to ASTM procedures (Table V).

TABLE II
BASIC NR RECIPE

Component	Loading, phr
NR SMR CV(60)	100
Carbon black	Varied
Zinc oxide	5
Stearic acid	3
Sulphur	2
TBBS	1

Downloaded from http://meridian.allenpress.com/rct/article-pdf/94/3/494/2908699/i0035-9475-94-3-494.pdf by Bureau of Science & Technology Information user on 06 October 2021

TABLE III
COMPOUNDING AND VULCANIZATION CONDITIONS[a]

Time, s	rpm	Operation
—	60	Load polymer
60	60	Ram down mixing
—	60	Load ½ CB, ZnO, and stearic acid
90	60	Ram down mixing
—	60	Load ½ CB
90	60	Ram down mixing (150 °C max, reduce rpm as necessary)
Total ~300	—	Discharge

[a] Banbury mixing pass: 70 °C, 60 rpm, 3 bar ram pressure. Curatives were added on two-roll mill: 70 °C, 25:21 rpm, gap 0.055–0.060 inches.

MEASUREMENT OF PAYNE EFFECT

Strain sweep measurements were made using an ARES rheometer with torsional parallel plate geometry. Successive dynamic strains from 0.1% to 62.5% single-strain amplitude were applied at 10 Hz to cylindrical samples (2 mm thickness × 8 mm diameter) around a zero mean strain. Cylindrical samples were bonded to the parallel plates using Loctite 480 adhesive, and a normal force control condition ensured that the cylinders remained under a slight compressive load during the whole procedure. Tests were performed at 60 °C and in duplicate.

FATIGUE CRACK GROWTH

The FCG behavior of the compounds was evaluated using a plane strain[38,39] test specimen measuring approximately 155 × 12.5 × 2 mm, into which an ~25-mm crack was cut with a razor blade. Before starting the crack growth test procedure, the specimen was cycled at the lowest applied fatigue displacement for 10 kcycles to precondition the crack tip. An MTS 831.10 elastomer test system was used to apply a 2.5 Hz sinusoidal fatigue displacement to the sample with a fully

TABLE IV
CB LOADING FOR 70 SHORE A ISO-HARDNESS COMPOUNDS

Carbon black	Iso-hardness loading, phr
N990	108
N772	63
N660	55
N550	50
N326	52
N330	47
N339	42
CB1	80
CB2	61
CB3	53
CB4	39
CB5	61

Downloaded from http://meridian.allenpress.com/rct/article-pdf/94/3/494/2908699/i0035-9475-94-3-494.pdf by Bureau of Science & Technology Information user on 06 October 2021

TABLE V
Basic Compound Property Test Methods

Test	Method reference	Temperature, °C
Mooney viscosity	34	100
Shore A hardness	35	23
Rebound resilience	36	23
Tensile stress–strain	37	23, 5× repeats

relaxing strain condition (R ratio = 0). At intervals of 2500 cycles during the fatigue process, the cyclic procedure was paused, and the specimen was strained to the peak displacement of the sinusoidal cycle to fully open the crack, then a length-calibrated image of the crack was captured using a Canon EOS Rebel T6 camera equipped with a macro lens. This process was repeated until a total crack growth of at least 0.5 mm had been achieved. This evaluation was repeated stepwise with increasing peak strain levels from ~15% up to ~50%, which was found to be sufficient to observe power law crack growth behavior in each compound. Tests were performed at room temperature. The crack growth rate at each strain level was determined from an analysis of crack length data obtained from the images using ImageJ software. The tearing energy (T) for plane strain specimens is given in Eq. 3 according to the energy balance approach of Rivlin and Thomas,[12] where a refers to the crack area, W refers to the strain energy density, and l_0 refers to the initial specimen height. In practical terms, the tearing energy was calculated using Eq. 4 to compensate for the reduction in specimen cross-sectional area due to progressive crack growth and for the non-zero strain energy of a volume of material in the cracked part of the specimen.[40] In Eq. 4, U is the strain energy, t_0 is the unstrained specimen thickness, w is the initial specimen width, c is the crack length, and e is a constant to account for the non-zero strain energy of the material in the cracked part of the specimen. The value of e is $0.28l_0$.[40] Testing was performed in duplicate. No major crack tip deviation/deflection was observed during the testing. Buckling/compression of the samples during testing was minimal.

The strain energy, U in Eq. 4, was calculated by integration of the mechanical force-displacement curve. Most published FCG work has used the integral of the mechanical unloading curve to calculate T. In this study, values of tearing energy were calculated from both loading curves (T_L) and the unloading curves (T_{UL}), and the contrast between the subsequent FCG results is discussed.

$$T = \left(\frac{dU}{da}\right)_l = W \cdot l_0 \tag{3}$$

$$T = \frac{U}{t_0(w - c + e)} \tag{4}$$

RESULTS AND DISCUSSION

BASIC COMPOUND PROPERTIES

Basic compound properties are reported in Table VI. The Shore A hardness of the compounds was consistent at about 70 ± 2 units. The Mooney viscosity values and rebound resilience values varied significantly within the compound set. The rebound resilience is related to the viscoelasticity of the compounds and can be correlated to the measured Payne effects and tanδ values.

Downloaded from http://meridian.allenpress.com/rct/article-pdf/94/3/494/2908699/i0035-9475-94-3-494.pdf by Bureau of Science & Technology Information user on 06 October 2021

TABLE VI
BASIC COMPOUND PROPERTIES

Property	N990	N772	N660	N550	N326	N330	N339	CB1	CB2	CB3	CB4	CB5
Shore A hardness	71	69	71	72	70	71	71	69	70	72	69	70
Mooney viscosity, MU	58.1	63.8	67.5	74.2	70.0	71.1	74.3	62.6	69.5	74.2	71.7	70.3
Rebound resilience, %	63.9	62.8	63.5	62.9	55.6	55.5	56.9	64.4	65.8	65.8	64	43.8
M25, MPa	1.61	1.46	1.62	1.81	1.45	1.46	1.43	1.34	1.65	1.61	1.47	1.43
M50, MPa	2.53	2.32	2.67	3.00	2.21	2.26	2.20	2.14	2.68	2.65	2.46	2.01
M100, MPa	5.01	4.67	5.35	5.79	4.32	4.61	4.48	4.30	5.44	5.31	4.90	3.45
M200, MPa	11.51	11.64	12.71	12.46	11.11	11.34	11.46	10.85	12.09	11.88	11.92	9.08
M300, MPa	14.41	18.17	19.02	18.1	19.03	18.55	19.62	17.37	17.94	17.7	19.22	16.32
Tensile strength, MPa	15.5	22.4	22.5	22.1	27.9	28.1	28.4	19.9	21.3	21.6	27.4	29.2
Elongation at break, %	338	393	362	382	430	451	429	347	379	376	420	492

Downloaded from http://meridian.allenpress.com/rct/article-pdf/94/3/494/2908699/i0035-9475-94-3-494.pdf by Bureau of Science & Technology Information user on 06 October 2021

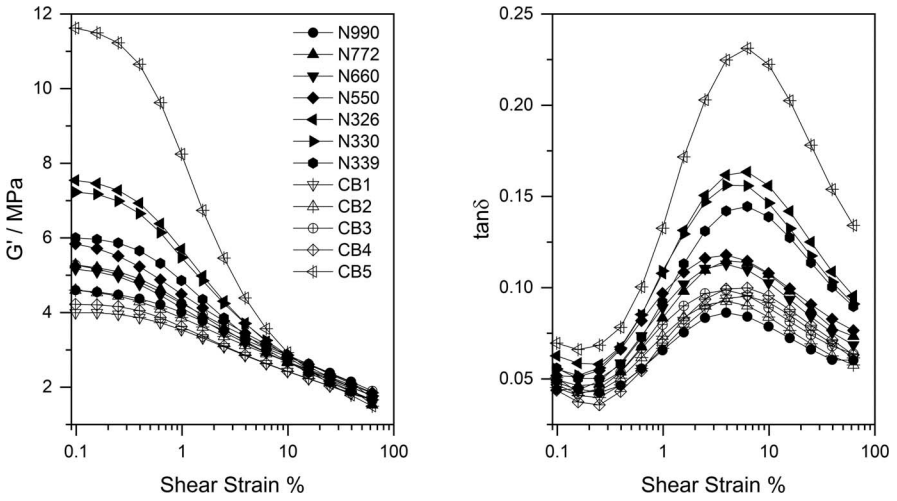

FIG. 4. — Payne effects of compounds measured at 60 °C.

The tensile moduli of the compounds over a range of strain percentage values are given in Table VI. Note that these moduli are defined per ASTM D412 as the tensile stress value at the indicated strain percentage (e.g., M50 is the tensile stress at 50% tensile strain). Also given in Table VI are the tensile strength and elongation at break values for each compound. The median value from the five repeats are reported for each parameter. The tensile moduli at each strain level were reasonably consistent over the full range of compounds, with 1σ standard deviation values for each strain level being approximately 10% of the mean value. The tensile failure properties of the compounds varied more significantly, with higher surface area CBs generally giving higher values for tensile strength and elongation at break.

PAYNE EFFECT RATIONALIZATION

Strain sweep data collected at 60 °C for each compound (G′ and tanδ as a function of shear strain) are plotted in Figure 4. Despite the compounds having reasonably similar static moduli, there are large variations in the measured strain-dependent dynamic moduli and tanδ depending on the type and loading of CB. The maximum observed tanδ value from the strain sweep experiments can be related to CB surface area by plotting versus the effective surface area of CB in the rubber compound. The effective surface area factor takes into account both the surface area and the loading of the CB in the compound and expresses the surface area of CB per gram of rubber in the final compound (Eq. 5). The resulting correlation is shown in Figure 5 and is consistent with the theory that CB primary particle size/surface area is the dominant parameter driving networking, hysteresis, and therefore heat buildup in rubber compounds. The inset in Figure 5 is a plot of $\tan\delta_{max}$ versus the corresponding drop in G′ over the examined strain range ($\Delta G' = G'_{0.1\%} - G'_{62.5\%}$), showing the direct correlation between these two features of the Payne effect.

$$SA_{eff} = \frac{STSA \times phr_{CB}}{phr_{rubber}} \quad (5)$$

Downloaded from http://meridian.allenpress.com/rct/article-pdf/94/3/494/2908699/i0035-9475-94-3-494.pdf by Bureau of Science & Technology Information user on 06 October 2021

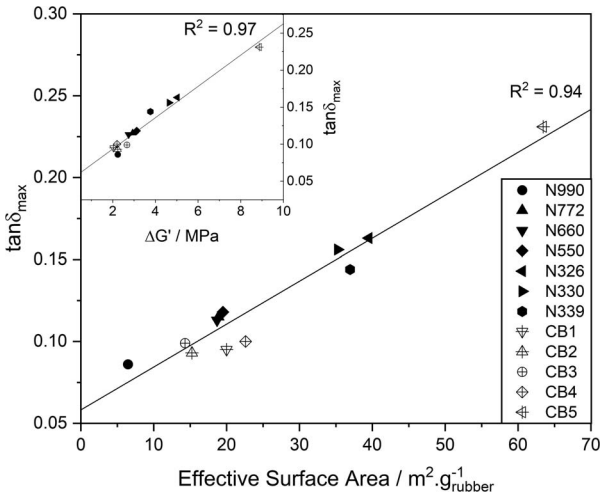

FIG. 5. — maximum from strain sweep data plotted versus the effective surface area of carbon black in the compounds. Inset: correlation of $\Delta G'$ parameter with $\tan\delta_{max}$.

ANALYSIS OF FCG PERFORMANCE OF ISO-HARDNESS COMPOUNDS

The FCG rates for the full set of compounds are plotted versus tearing energy in Figure 6. The crack growth data are plotted versus tearing energies calculated from both the mechanical loading (red data sets) and unloading curves (black data sets). The FCG behavior of all compounds are well described by a power law relation between crack growth rate and tearing energy (Eq. 2). The values of the crack growth rate law parameters for each material with tearing energy calculated from both the loading (T_L) and unloading (T_{UL}) force-deflection curve along with R^2 values are presented in Table VII. There are clear differences in the crack growth behavior of compounds depending on the CB type. The key difference is the slopes of the crack growth data sets (β) and a horizontal shifting of the data sets depending on the methodology used to define the tearing energy. Note that the β values are broadly independent of the methodology used to define the tearing energy. The β values reported here span a range between 1.54 and 3.32, with a mean value of 2.22. Typical average values of β reported in the classical literature for CB reinforced NR are $\sim$2.[1] Recently, more substantial deviations from this value have also been reported.[41]

These data can be rationalized by considering microstructural factors contributing to crack growth resistance. For NR compounds, a major toughening effect arises from SIC of a portion of the highly strained rubber directly ahead of the crack tip. Anisotropic NR crystallites form under high-straining conditions and are orientated along the stretching direction (i.e., orthogonal to the direction of crack growth). This effect has been studied extensively, and it results in both a masking of the viscoelastic, T_g-driven toughening effects seen in non–strain crystallizing rubbers as well as increases in crack tip deflection and consequently compound tear resistance.[1,4,19] The presence of CB in NR compounds reduces the global strains required for the onset of crystallization through localized strain amplification, leading to a toughening of filled compounds versus the unfilled rubber.

Calculations of the levels of strain amplification in CB-reinforced rubber from the first principles rely on knowledge of the volume fraction of CB in the compound. Simple volume fraction approaches are complicated by the complex aggregate structure of CBs, the high loading levels typically used in rubber applications, and the tendency of CB aggregates to network/agglomerate within in the rubber compound.[42–44] At small to medium strain levels, networking of

Downloaded from http://meridian.allenpress.com/rct/article-pdf/94/3/494/2908699/i0035-9475-94-3-494.pdf by Bureau of Science & Technology Information user on 06 October 2021

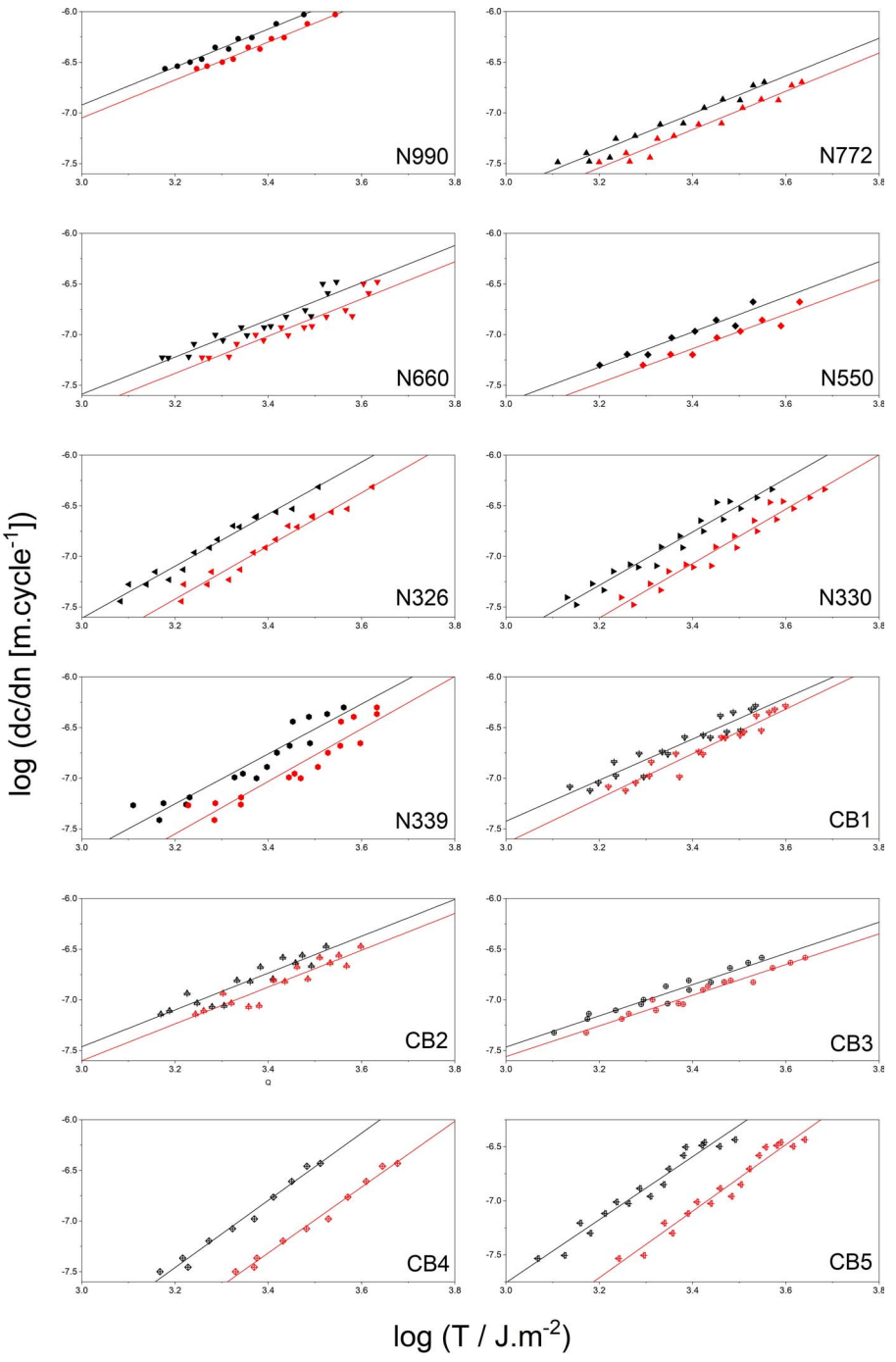

FIG. 6. — Logarithm of fatigue crack growth rate data for each compound plotted versus logarithm of tearing energy. Red data sets are from tearing energies calculated from mechanical loading curves; black data sets are from tearing energies calculated from mechanical unloading curves.

Downloaded from http://meridian.allenpress.com/rct/article-pdf/94/3/494/2908699/i0035-9475-94-3-494.pdf by Bureau of Science & Technology Information user on 06 October 2021

TABLE VII
FCG POWER LAW PARAMETERS AND STRAIN AMPLIFICATION FACTORS

Carbon black	T_{UL}			T_L			Strain amplification, X
	β	log(A)	R^2	β	log(A)	R^2	
N990	1.87	−12.55	0.98	1.87	−12.67	0.98	3.90
N772	1.94	−13.33	0.96	1.89	−13.59	0.96	3.30
N660	1.83	−13.09	0.90	1.83	−13.25	0.90	3.29
N550	1.73	−12.86	0.92	1.70	−12.91	0.92	3.25
N326	2.57	−15.32	0.97	2.62	−15.83	0.96	3.09
N330	2.63	−17.70	0.96	2.68	−16.20	0.95	3.22
N339	2.46	−15.13	0.89	2.59	−15.84	0.88	3.13
CB1	2.03	−13.51	0.91	2.20	−14.25	0.93	3.30
CB2	1.82	−12.91	0.86	1.82	−13.10	0.87	3.40
CB3	1.54	−12.09	0.94	1.51	−12.10	0.96	3.43
CB4	3.32	−18.07	0.98	3.25	−18.36	0.99	2.93
CB5	2.91	−16.50	0.95	3.08	−17.56	0.96	3.01

filler aggregates must be accounted for. To this end, a strain amplification model considering strain-dependent overlapping fractal clusters has been developed and implemented.[45,46] For the analysis of FCG data, it is important to consider the highly strained region of rubber immediately ahead of the crack tip. Under such high-strain conditions, it is proposed here that CB aggregate networking is minimized and the levels of strain amplification can be more simply described by hydrodynamic equations derived from the Einstein viscosity equation, such as the well-known Guth–Gold equation.[47,48] Accordingly, strain amplification factors for each compound in this study were calculated following the approach of Mullins and Tobin,[49] who defined a strain amplification factor, X, relating the global applied strain, ε_g, to the average local strain in the rubber, ε_l (Eq. 6). Mullins and Tobin used the Guth–Gold equation (Eq. 7) to define X. Values of X for each compound are presented in Table VII.

$$\varepsilon_l = X\varepsilon_g \tag{6}$$

$$X = 1 + 2.5\varphi_{\text{eff}} + 14.1\varphi_{\text{eff}}^2 \tag{7}$$

In Eq. 7, the effective volume fraction, φ_{eff}, is defined as the volume fraction of the CB in the compound plus the volume fraction of rubber shielded or occluded from global strains by the CB aggregate structure. The volume fraction of CB in the compounds, φ, is defined in Eq. 8, where the density of CB is taken as 1.81 g/cm^3 and the density of NR is taken as 0.92 g/cm^3. For simplicity, Eq. 8 ignores the contribution from curatives in the formulation. The effective volume fraction can be calculated in a number of ways, for example, simply calculated from the void volume data generated from quantitative transmission electron microscopy structure analysis of CB aggregates[50] or derived from the fractal scaling law of the aggregates.[51,52] In this work, however, the effective volume fraction is calculated from Eq. 9 using the actual volume fraction of CB, φ, and the COAN structure values of the CBs via the approach originally outlined by Medalia[53] and later modified by Wang et al.[54] Equation 9 is derived by considering the oil absorption test results to be a function of the volume of occluded oil within aggregates. The full assumptions and derivation of Eq. 9 are given in Appendix A.

Downloaded from http://meridian.allenpress.com/rct/article-pdf/94/3/494/2908699/i0035-9475-94-3-494.pdf by Bureau of Science & Technology Information user on 06 October 2021

Analysis of recently published experimental data by Liu et al.[55] suggests that this approach (i.e., Eqs. 6–9) is suitable for a quantitative description of the state of strain of rubber ahead of crack tips (see Appendix B for further discussion).

$$\varphi = \frac{\left(\frac{\text{phr}_{CB}}{\rho_{CB}}\right)}{\left(\frac{\text{phr}_{CB}}{\rho_{CB}}\right) + \left(\frac{\text{phr}_{NR}}{\rho_{NR}}\right)} \tag{8}$$

$$\varphi_{eff} = \varphi\left(\frac{0.0181\text{COAN} + 1}{1.59}\right) \tag{9}$$

Figure 7A–D plots the linearized FCG power law parameters versus the calculated strain amplification factors for each compound. Figure 7A–B show data in which tearing energy has been calculated from mechanical unloading force-deflection data. Figure 7C–D shows data in which tearing energy has been calculated from mechanical loading force-deflection data.

An excellent correlation exists between the power law parameters and calculated strain amplification factors, independent of the method of calculation of the tearing energy. Increasing strain amplification is correlated with a drop in the crack growth exponent, β, meaning that the crack growth rate becomes less sensitive to changes in applied tearing energy. Accordingly, there is a concomitant increase of the intercept parameter, log(A). This provides a quantitative link between key properties of CBs and the theory that a major contribution to CBs' enhancement of crack growth resistance in NR compounds is through the promotion of localized SIC via strain amplification. The fact that the Guth–Gold equation is successful in scaling the FCG data suggests that networking of aggregates in the highly strained region ahead of the crack tip is minimal. Note that there is some discussion in the literature as to the correct value for the second coefficient term in the Guth–Gold series expansion and to the general applicability of such equations at large strains and high filler loadings.[56,57] In light of this, it is worthwhile to point out that the corrected values for the second coefficient found in the literature (for example, 5.2,[58] 5.01,[59,60] etc.) scale the FCG data equally as well as Eq. 7 does. Strain amplification is also well-known to control the static mechanical moduli of rubber compounds.[61] As such, increases in compound stiffness through increased CB loading and structure levels may be expected to correlate to systematic changes in FCG behavior.

An obvious exception to the correlations obtained in Figure 7A–D is the N990-reinforced compound. This compound shows far worse FCG resistance than is predicted by the calculated strain amplification factor. This could potentially be due to the debonding of rubber from the surface of the large particle size N990 aggregates during fatigue loadings, or this may indicate a practical upper limit to the strain amplification scaling of FCG behavior. Further investigation on this point is needed.

It is also necessary to consider the role of CB-induced hysteresis in crack growth resistance. Figure 8 shows an example load-deflection data from data sets for the N990 and CB5 compounds. These data were collected after 10^4 strain cycles to 2.75 mm peak deflection. N990 and CB5 have the lowest and highest surface area values of the CBs examined and therefore the greatest contrast in compound hysteresis. Although the initial stiffness upon loading is equivalent between the two compounds, the unloading curves show significant differences arising because of the inherent differences in surface area–driven hysteresis. The implication here is that although T_L and T_{UL} values will not differ significantly for the N990 compound, a much greater distinction between tearing energies for more hysteretic compounds such as CB5 will be apparent. To illustrate this point, the crack growth rate data for N990 and CB5 compounds is plotted versus both T_L and T_{UL} values in Figure 9. Note that the β parameters are substantially unaffected by tear energy calculation methodology; in fact, this observation is consistent across the entire range of compounds studied

Downloaded from http://meridian.allenpress.com/rct/article-pdf/94/3/494/2908699/i0035-9475-94-3-494.pdf by Bureau of Science & Technology Information user on 06 October 2021

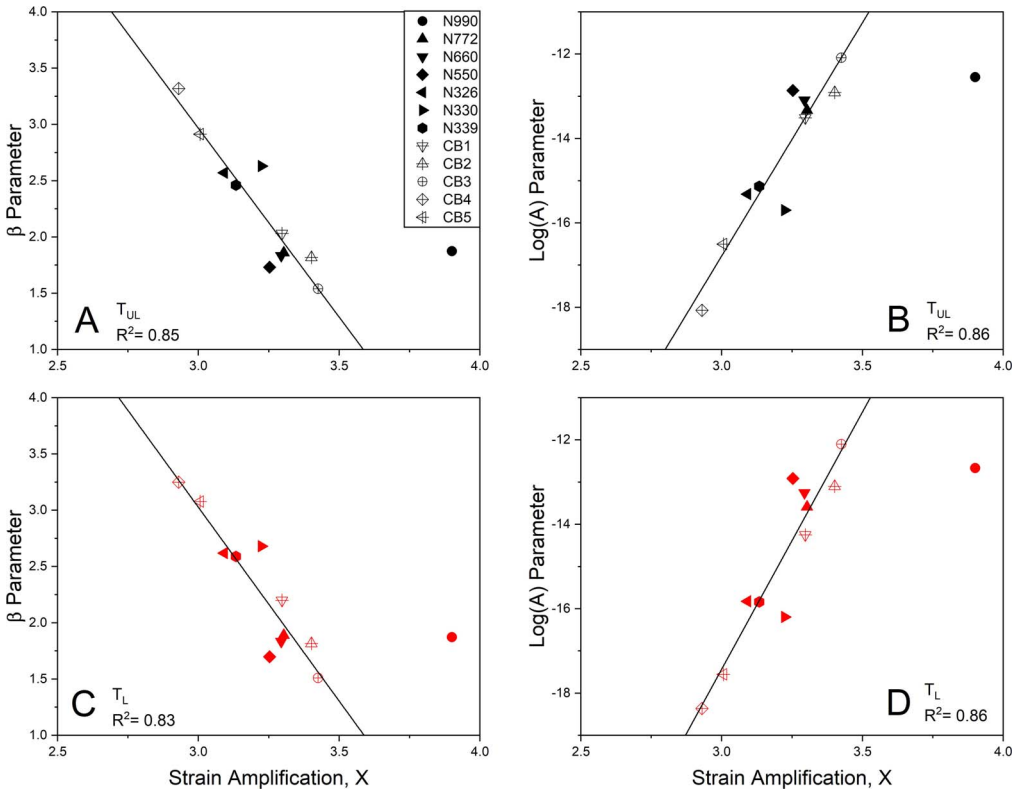

FIG. 7. — Plots of (A) β parameter versus strain amplification factor, T_{UL} data. (B) log(A) parameter versus strain amplification factor, T_{UL} data. (C) β parameter versus strain amplification factor, T_L data. (D) log(A) parameter versus strain amplification factor, T_L data.

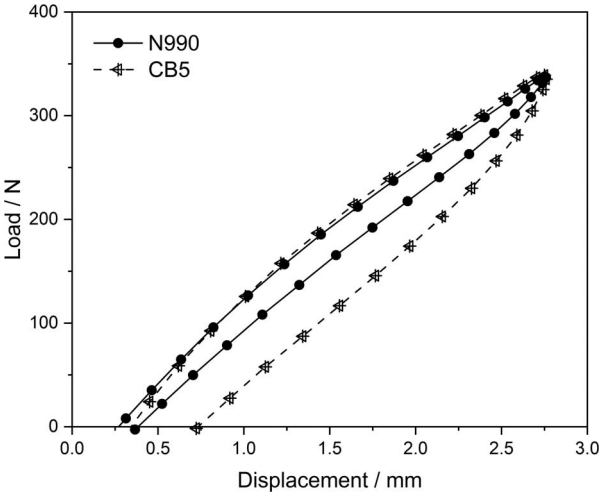

FIG. 8. — Example cyclic load-displacement data for N990 and CB5 compounds taken from the raw FCG test data.

Downloaded from http://meridian.allenpress.com/rct/article-pdf/94/3/494/2908699/i0035-9475-94-3-494.pdf by Bureau of Science & Technology Information user on 06 October 2021

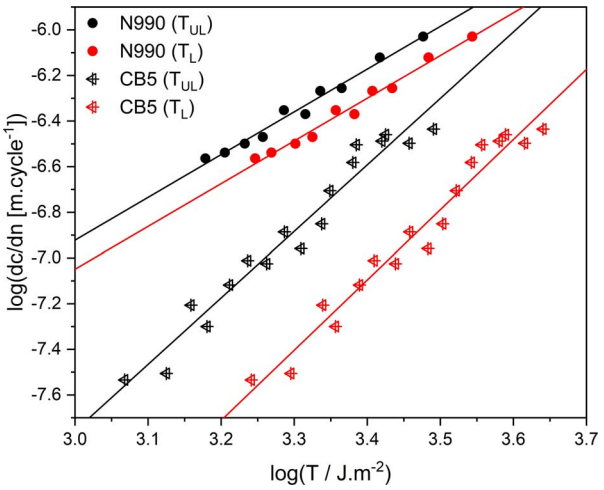

FIG. 9. — FGC behavior for N990 and CB5 compounds plotted verses T_L and T_{UL} values.

(Table VII and Figure 6). The more hysteretic CB5 compound undergoes a significant horizontal shifting in FCG data when the dissipated energy is included in the tear energy calculation (i.e., T_L). This is a systematic effect that can be illustrated when the differences between log(A) parameters from the two tear energy calculation methods are plotted versus the CB effective surface area in each compound in Figure 10 (recall that the CB effective surface area factor is the primary driver of networking and hysteresis in these compounds, as demonstrated in Figure 5). The CB1 data point seems to be an obvious outlier from an otherwise linear correlation.

From this data set and subsequent analyses, it is apparent that

1. Strain amplification and SIC control the slope of the crack growth law on a log–log axis (i.e., β parameter).
2. Compound hysteresis contributes to the horizontal positioning of the power law crack growth data (i.e., log(A) parameter).

These observations highlight some interesting tearing energy–dependent conflicts for FCG performance and CB selection. This is illustrated by considering the FCG data sets of CB3 and CB5 compounds. The CB3 compound has one of the highest calculated levels of strain amplification in this study, whereas CB5 has one of the lowest. Figure 11 plots the FCG data for both T_L and T_{UL} for each compound. Calculated values of X and SA_{eff} for each compound are indicated in the figure. The data sets for the two compounds exhibit a crossover in terms of crack growth performance irrespective of whether T_L or T_{UL} is used. This indicates that at lower tearing energies, the levels of compound hysteresis dominate crack growth resistance, whereas at higher tearing energies (approaching T_c), it is the levels of strain amplification that dominate performance. This would seem reasonable, because crack tip SIC would be more prevalent under more severe straining conditions. Therefore, a conflict in CB selection exists between achieving good crack growth resistance at lower tearing energies versus high tearing energies for situations in which iso-hardness conditions are required (e.g., a narrow specification window for compound static stiffness).

Finally, it is worth considering the well-known effects of CB properties on the critical tear energy, T_c. At equal loading and particle size of CB, increasing the CB structure increases both the stiffness/moduli of the rubber compound and decreases the measured T_c. This decrease in T_c has

Downloaded from http://meridian.allenpress.com/rct/article-pdf/94/3/494/2908699/i0035-9475-94-3-494.pdf by Bureau of Science & Technology Information user on 06 October 2021

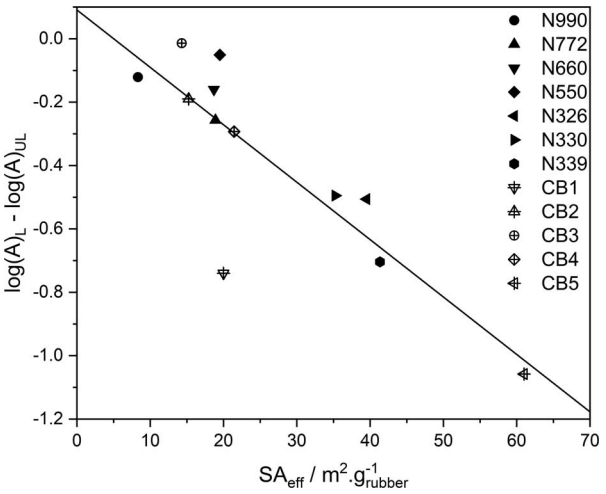

FIG. 10. — Difference in power law log(A) parameters determined from T_L and T_{UL} values versus compound effective CB surface area. The CB1 data point was excluded from the linear regression.

been proposed to be related to a sharpening of the crack tip due to the enhancement in compound stiffness, which reduces the volume of highly strained rubber ahead of the crack and seemingly overwhelms any structure-driven promotion of SIC.[20,62,63] This implies a performance tradeoff when attempting to optimize for FCG and T_c performance. The compounds studied in this work were prepared to iso-hardness conditions. As such, the stress–strain behaviors of all the compounds were broadly comparable. If, on the other hand, compounds were prepared to iso-loadings, the stress–strain behavior of the compounds would vary dramatically depending on the structure levels of the CBs. Therefore, under conditions in which stress–strain behaviors are dramatically different between compounds, we could perhaps anticipate a more complex interplay between FCG behavior and CB structure.

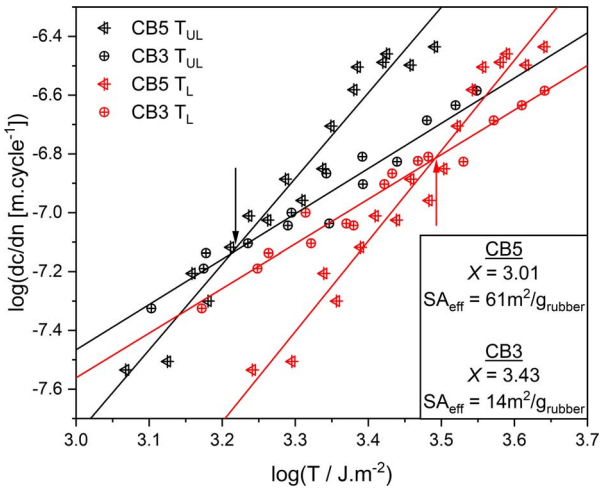

FIG. 11. — FCG data for CB3 and CB5 (T_L and T_{UL} data sets) exhibiting crossover behavior in crack growth behavior as indicated by arrows.

Downloaded from http://meridian.allenpress.com/rct/article-pdf/94/3/494/2908699/i0035-9475-94-3-494.pdf by Bureau of Science & Technology Information user on 06 October 2021

FUTURE EXTENSIONS OF THIS WORK

The results of this study provide evidence that the FCG performance of reinforced NR can be rationalized in terms of simple concepts related to the type and loading of CB. However, substantial additional experiments and data analyses are required to confirm and extend these concepts. Proposed follow-up work to this study involves conducting similar experiments in NR at iso-loading of CB over a range of different loading levels. In this case, the static stiffness will vary greatly between compounds depending on the type of CB, which may result in differences in the shape and diameter of the crack tip between compounds.[20,62,63] Furthermore, experiments performed on reinforced NR compounds under nonrelaxing conditions (i.e., where crystallites at the crack tip persist throughout the entirety of the FCG experiments) could be expected to display a strong dependence on calculated values of *X*. In addition, analogous iso-loading and iso-hardness testing performed in a non–strain crystallizing rubber with a T_g similar to that of NR, such as emulsion SBR, would be very helpful for contrasting the effects of strain amplification in crystallizing and noncrystallizing rubbers. Although strain amplification is seemingly beneficial in crystallizing rubbers, this may not necessarily be the case for non-SIC rubbers. Consequently, there may be performance consequences for blends of SIC and non-SIC rubbers, dependent on blending ratios. In addition, direct characterization of the actual levels of strain amplification in the rubber compounds from complimentary experimental techniques would also be revealing.[64]

As described in the introduction to this work, FCG behavior only partially defines the fatigue life of rubber components. It will be necessary to consolidate learnings from these experiments with knowledge of crack precursor size and precursor distributions in rubber compounds[65] to quantitatively describe and predict the results of fatigue life experiments.

CONCLUSION

FCG behaviors were evaluated for 12 NR compounds reinforced with various CBs and prepared to a Shore A hardness of 70. In the resulting FCG data sets, significant variations in the β exponent of the power law FCG behavior were observed. These variations were rationalized by assuming that the highly strained state of the rubber compound ahead of the crack tip effectively minimizes CB aggregate networking and allows for the application of hydrodynamic concepts to calculate realistic strain amplification factors. With one exception, a good scaling of FCG behavior to the calculated strain amplification factors was observed. This scaling is likely underpinned by the promotion of SIC ahead of the crack tip through localized strain amplification. Contrasting the results obtained from tearing energies calculated by using the mechanical loading data as well as unloading data provided some insight into the role of compound hysteresis (driven primarily by CB surface area) in FCG performance. The findings presented here provide quantitative insights into the physical mechanisms underlying crack growth resistance of CB-reinforced NR. From a practical standpoint, the potential ability to rank FCG performance of various CBs a priori from knowledge of the structure level and compound formulation loading could be a useful tool for improved design of rubber compounds. Future work to verify these findings and extend the concepts explored in this article has been outlined.

ACKNOWLEDGEMENTS

The author is grateful to Birla Carbon for granting permission to publish this work.

REFERENCES

[1]M. D. Ellul, Chapter 6, in "Engineering with Rubber: How to Design Rubber Components," A. N. Gent, Ed., Carl Hanse Verlag, Munich, 1992.

Downloaded from http://meridian.allenpress.com/rct/article-pdf/94/3/494/2908699/i0035-9475-94-3-494.pdf by Bureau of Science & Technology Information user on 06 October 2021

[2]A. G. Thomas, *J. Polym. Sci*. **31**, 467 (1958).

[3]A. N. Gent, P. B. Lindley, and A. G. Thomas, *J. Appl. Polym. Sci*. **8**, 455 (1964) [reprinted in RUBBER CHEM. TECHNOL. **38**, 301 (1965)].

[4]W. V. Mars and A. Fatemi, RUBBER CHEM. TECHNOL. **77**, 391 (2002).

[5]W. V. Mars and A. Fatemi, *Int. J. Fatigue* **24**, 949 (2002).

[6]J. B. Le Cam, B. Huneau, E. Verron, and L. Gornet, *Macromolecules* **37**, 5011 (2004).

[7]B. Huneau, I. Masquelier, Y. Marco, V. Le Saux, S. Noizet, C. Schiel, and P. Charrier, RUBBER CHEM. TECHNOL. **89**, 126 (2016).

[8]B. N. J. Persson, O. Albohr, G. Heinrich, and H. Ueba, *J. Phys. Condens. Matter* **17**, R1071 (2008).

[9]C. G. Robertson, R. Stoček, and V. W. Mars, "The Fatigue Threshold of Rubber and Its Characterization Using the Cutting Method," in *Advances in Polymer Science*, Springer, New York, 2020.

[10]C. G. Robertson, R. Stoček, C. Kipscholl, and V. W. Mars, *Tire Sci. Technol*. **47**, 292 (2019).

[11]A. A. Griffith, *Phil. Trans*. **A221**, 163 (1920).

[12]R. S. Rivlin and A. G. Thomas, *J. Polym. Sci*. **10**, 291 (1953).

[13]G. J. Lake and O. H. Yeoh, *Int. J. Fracture* **14**, 509 (1978).

[14]A. K. Bhowmick, *J. Macromol. Sci. Part C: Polym. Rev*. **28**, 339 (1988).

[15]A. Kadir and A. G. Thomas, RUBBER CHEM. TECHNOL. **54**, 15 (1981).

[16]K. Tsunoda, J. J. C. Busfield, C. K. L. Davies, and A. G. Thomas, *J. Mater. Sci*. **35**, 5187 (2000).

[17]R. Stoček, "Some Revisions of Fatigue Crack Growth Characteristics of Rubber," in *Advances in Polymer Sciences*, Springer, New York, 2020.

[18]P. B. Lindley, *Int. J. Fracture* **9**, 449 (1973).

[19]K. Brüning, K. Schneider, S. V. Roth, and G. Heinrich, *Macromolecules* **45**, 7914 (2012).

[20]J.-B. Donnet, R. C. Bansal, and M. J. Wang, Eds., *Carbon Black: Science and Technology,* 2nd ed. Marcel Dekker, New York, 1993.

[21]C. R. Herd, G. C. McDonald, and W. M. Hess, RUBBER CHEM. TECHNOL. **66**, 491 (1993).

[22]A. I. Medalia, *J. Colloid Interface Sci*. **32**, 115 (1970).

[23]ASTM Standard D6556-19a "Standard Test Method for Carbon Black—Total and External Surface Area by Nitrogen Adsorption" *Annu. Book ASTM Stand*. **09.01** (2019).

[24]ASTM Standard D2414-19, "Standard Test Method for Carbon Black–Oil Absorption Number (OAN)," *Annu. Book ASTM Stand*. **09.01** (2019); ASTM Standard D3493-19a, "Standard Test Method for Carbon Black–Oil Absorption Number of Compressed Sample (COAN)," *Annu. Book ASTM Stand*. **09.01** (2019).

[25]G. J. Lake and P. B. Lindley, *Rubber J*. **146**, 30 (1964).

[26]C. M. Roland, "Reference Module in Materials Science and Engineering," 2016, http://polymerphysics.net/pdf/Reinforcement%20of%20Elastomers%202016.pdf. Accessed date February 29, 2020.

[27]M. Rowlinson, C. R. Herd, G. Moninot, N. Thomas, and J. A. Ayala, *Kaut. Gummi Kunst*. **52***,* 830 (1999).

[28]K. Reincke, W. Grellmann, and M. Klüppel, *Kaut. Gummi Kunst*. **5**, 246 (2009).

[29]M. Wunde and M. Klüppel, RUBBER CHEM. TECHNOL. **91**, 668 (2018).

[30]H. Sridharan, J. Chanda, P. Ghosh, and R. Mukhopadhyay, RUBBER CHEM. TECHNOL. **92**, 415 (2019).

[31]J. M. Pilarski, J. R Goossens, W. V. Mars, and C. G. Robertson, *Constitutive Models for Rubber XI: Proceedings of the 11th European Conference on Constitutive Models for Rubber (ECCMR 2019)*, Jun 25–27, 2019, Nantes, France, CRC Press, 2019.

[32]S. Toki, I. Sics, S. F. Ran, L. Z. Liu, B. S. Hsiao, S. Murakami, K. Senoo, and S. Kohjiya, *Macromolecules* **35**, 6578 (2002).

[33]H. W. Greensmith, *J. Appl. Polym. Sci*. **3**, 175 (1960).

[34]ASTM Standard D1646-19a, "Standard Test Method for Rubber—Viscosity, Stress Relaxation, and Pre-vulcanization Characteristics (Mooney Viscometer)," *Annu. Book ASTM Stand*. **09.01** (2019).

Downloaded from http://meridian.allenpress.com/rct/article-pdf/94/3/494/2908699/i0035-9475-94-3-494.pdf by Bureau of Science & Technology Information user on 06 October 2021

[35]ASTM Standard D2240-15e1, "Standard Test Method for Rubber Property—Durometer Hardness," *Annu. Book ASTM Stand*. **09.01** (2015).

[36]ASTM Standard D7121-05, "Standard Test Method for Rubber Property—Resilience Using Schob Type Rebound Pendulum," *Annu. Book ASTM Stand*. **09.01** (2018).

[37]ASTM Standard D412-16, "Standard Test Method for Vulcanized Rubber and Thermoplastic Elastomers—Tension," *Annu. Book ASTM Stand*. **09.01** (2016).

[38]R. Stoček, M. Stěnička, and J. Maloch, "Determining Parametrical Functions Defining the Deformations of a Plane Strain Tensile Rubber Sample," in *Advances in Polymer Science*, Springer, New York, 2020.

[39]J. S. Bergstrom, *Mechanics of Solid Polymers*. Elsevier, London, 2015.

[40]J. J. C. Busfield, C. H. H. Ratsimba, and A. G. Thomas, *J. Nat. Rubber Res*. **12**, 131 (1997).

[41]R. Stoček, G. Heinrich, M. Gehde, and R. Kipscholl, "Analysis of Dynamic Crack Propagation in Elastomers by Simultaneous Tensile and Pure-Shear Mode Testing," in *Fracture Mechanics and Statistical Mechanics of Reinforced Elastomeric Blends: Lecture Notes in Applied and Computational Mechanics*, W. Grellmann, G. Heinrich, M. Kaliske, M. Klüppel, K. Schneider, and Th.A. Vilgis, Eds., Springer, Berlin, 2013, pp. 269–301.

[42]L. B. Tunnicliffe, J. Kadlcak, M. D. Morris, Y. Shi, A. G. Thomas, and J. J. C. Busfield, *Macromol. Matter. Eng*. **299**, 12 (2014).

[43]L. B. Tunnicliffe, A. G. Thomas, and J. J. C. Busfield, *Macromol. Matter. Eng*. **301**, 1202 (2016).

[44]L. B. Tunnicliffe and J. J. C. Busfield, *Adv. Polym. Sci*. **275**, 71 (2016).

[45]G. Huber and T. A. Vilgis, *Kaut. Gummi Kunst*. **52**, 102 (1999).

[46]M. Klüppel, *Adv. Polym. Sci*. **164**, 1 (2003).

[47]E. Guth and O. Gold, *Phys. Rev*. **53**, 322 (1938).

[48]E. Guth, RUBBER CHEM. TECHNOL. **18**, 596 (1945).

[49]L. Mullins and N. R. Tobin, RUBBER CHEM. TECHNOL. **39**, 799 (1966).

[50]ASTM D3849-14a, "Standard Test Method for Carbon Black—Morphological Characterization of Carbon Black Using Electron Microscopy," *Annu. Book ASTM Stand*. **09.01** (2014).

[51]C. R. Herd, G. C. McDonald, and W. M Hess, RUBBER CHEM. TECHNOL. **65**, 107 (1992).

[52]G. Heinrich and M. Klüppel, RUBBER CHEM. TECHNOL. **68**, 623 (1995).

[53]A. I. Medalia, RUBBER CHEM. TECHNOL. **45**, 1172 (1972).

[54]M. J. Wang, S. Wolff, and E. H. Tan, RUBBER CHEM. TECHNOL. **66**, 178 (1993).

[55]C. Liu, B. Dong, L. Q. Zhang, Q. Zheng, and Y. P. Wu, RUBBER CHEM. TECHNOL. **88**, 276 (2015).

[56]G. Allegra, G. Raos, and M. Vacatello, *Prog. Polym. Sci*. **33**, 683 (2008).

[57]J. Domurath, M. Saphiannikova, and G. Heinrich, *Kautsch. Gummi. Kunstst*. **1–2**, 40 (2017).

[58]G. G. Batchelor and J. T. Green, *J. Fluid Mech*. **56**, 401 (1972).

[59]H. S. Chen and A. Acrivos, *Int. J. Solids Struc*. **14**, 331 (1978).

[60]H. S. Chen and A. Acrivos, *Int. J. Solids Struc*. **14**, 349 (1978).

[61]G. Kraus, RUBBER CHEM. TECHNOL. **44**, 199 (1971).

[62]A. G. Thomas, *J. Polym. Sci*. **18**, 177 (1955).

[63]H. W. Greensmith, *J. Polym. Sci*. **21**, 175 (1956).

[64]R. Pérez-Aparicio, M. Schiewek, J. L. Valentín, H. Schneider, D. R. Long, M. Saphiannikova, P. Sotta, K. Saalwächter, and M. Ott, *Macromolecules* **46**, 5549 (2013).

[65]C. G. Robertson, L. B. Tunnicliffe, L. Maciag, M. Bauman, K. Miller, C. R. Herd, and W. V. Mars, *Polymers* **12**, 203 (2020).

[66]ASTM D1765-14, "Standard Classification System for Carbon Blacks Used in Rubber Products," *Annu. Book ASTM Stand*. **09.01** (2014).

[*Received July 2020, Revised March 2021*]

Downloaded from http://meridian.allenpress.com/rct/article-pdf/94/3/494/2908699/i0035-9475-94-3-494.pdf by Bureau of Science & Technology Information user on 06 October 2021

APPENDIX A: DERIVATION OF EFFECTIVE VOLUME FRACTION EQUATION

Wang et al.[54] derived Eq. 9 by building on the earlier work of Medalia,[22,53] which considered that the endpoint of the oil absorption titration of CB can be described as follows: a specific volume of oil has completely filled the space between the branches of the individual aggregates. As such, the aggregates in the oil/CB cake at the end of the test can be assumed to exist as nonoverlapping equivalent spheres. An additional volume of oil also fills the gaps between these packed, equivalent spheres. These intra-aggregate and interaggregate oil volumes can then be deconvoluted. The permeated equivalent sphere volume and interaggregate oil volume are calculated by assuming that the equivalent spheres pack randomly at a volume fraction of 0.63[40] (the average of cubic and face centered maximum packing fractions). The effective volume fraction in a rubber compound is then given by Eqs. 10–12, where V_p is the permeated volume of equivalent spheres, V_f is the volume of filler, V_v is the volume between the permeated equivalent spheres, and ρ_{CB} is the density of the CB. Assuming ρ_{CB} of 1.81 g.cm^{-3}, this reduces to Eq. 9.

$$\varphi_{\text{eff}} = \varphi\left(\frac{1+e}{1+\epsilon}\right) \tag{10}$$

$$e = \frac{(V_p - V_f) + V_v}{V_f} = \frac{\rho_{CB}\text{COAN}}{100} \tag{11}$$

$$\epsilon = \frac{V_v}{V_p} = \frac{0.37}{1-0.37} \tag{12}$$

APPENDIX B: STRAIN AMPLIFICATION AHEAD OF CRACK TIPS

Recently, Liu et al.[55] presented an experimental characterization of the state of strain of rubber just ahead of crack tips using a digital image correlation technique. They investigated four types of CB: N990, N660, N330, and N234, each loaded at 50 phr in a sulfur vulcanized SBR compound. They reported the maximum strain of the rubber directly ahead of the crack tip in single-edged notched tension specimens under various global strain, ε_g, conditions for each compound. Their data are reproduced in Appendix Table I. These global and local strain data are converted into experimentally determined strain amplification factors, X, using Eq. 6 of this article. These X values are also presented in Appendix Table I in parentheses. Theoretical strain amplification factors can

APPENDIX TABLE I
LOCAL CRACK TIP AND GLOBAL STRAIN DATA REPRODUCED FROM LIU ET AL.[55a]

	Local strain at crack tip (strain amplification factor)			
Global strain, ε_g	N234	N330	N660	N990
0.3	0.98 (3.27)	1.01 (3.37)	0.99 (3.30)	0.84 (2.80)
0.5	1.84 (3.68)	1.88 (3.76)	1.36 (2.72)	1.39 (2.78)
0.7	2.65 (3.79)	2.51 (3.59)	2.09 (2.99)	1.72 (2.46)
0.9	3.40 (3.78)	3.04 (3.38)	2.69 (2.99)	2.23 (2.48)
1.0	3.75 (3.75)	3.36 (3.36)	2.96 (2.96)	2.35 (2.35)

[a] Calculated strain amplification factors appear in parentheses.

Downloaded from http://meridian.allenpress.com/rct/article-pdf/94/3/494/2908699/i0035-9475-94-3-494.pdf by Bureau of Science & Technology Information user on 06 October 2021

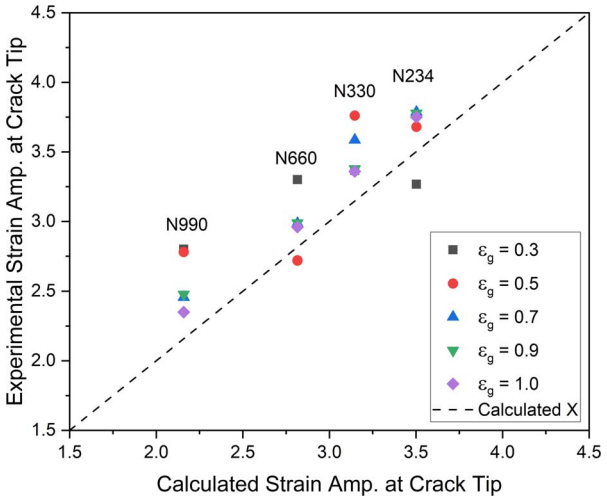

APPENDIX FIG. 1. — Plot of experimentally determined strain amplification factors ahead of the crack tip from data of Liu et al.[55] versus calculated strain amplification factors.

be calculated using Eqs. 7 and 9 of this article. To do this, typical values for COAN of the CBs used by Liu et al.[55] were assumed.[66] Appendix Figure 1 shows a plot of the experimental strain amplification factors determined by Liu et al. versus calculated values for a range of applied global strain levels. A good agreement between experimental and calculated values is found. This is evidence that the state of strain amplification ahead of crack tips in rubber compounds can be reasonably described using the approached outlined in this paper.

Downloaded from http://meridian.allenpress.com/rct/article-pdf/94/3/494/2908699/i0035-9475-94-3-494.pdf by Bureau of Science & Technology Information user on 06 October 2021